Excited state nonadiabatic dynamics of bare and hydrated anionic gold clusters Au_3^- $[H_2\ O]_n$ (n =0-2)

Polina G. Lisinetskaya and Roland Mitrić

Institut für Physikalische und Theoretische Chemie, Universität Würzburg, D-97074 Würzburg, Germany

Christian Braun, Sebastian Proch, and Gerd Ganteför

Fachbereich Physik, Universität Konstanz, D-78464 Konstanz, Germany

Young Dok Kim

Department of Chemistry, Sungkyunkwan University, 440-746 Suwon, Republic of Korea

Abstract

We present a joint theoretical and experimental study of the excited state dynamics in pure and hydrated anionic gold clusters Au_3^- $[H_2\ O]_n$ (n=0-2). We employ mixed quantum-classical dynamics combined with femtosecond time-resolved photoelectron spectroscopy in order to investigate the influence of hydration on excited state lifetimes and the photo-dissociation dynamics. Gradual decrease of the excited state lifetime with the number of adsorbed water molecules as well as gold cluster fragmentation quenching by two or more water molecules are observed both in experiment and in simulations. Non-radiative relaxation and dissociation in excited states are found to be responsible for the excited state population depletion. Time constants of these two processes strongly depend on the number of water molecules leading to the possibility to modulate excited state dynamics and fragmentation of the anionic cluster by adsorption of water molecules.

I. INTRODUCTION

Nano- and sub-nanosized noble metal clusters and their aggregates are in the focus of interest due to their unique optical, chemical, and electronic properties as compared to bulk materials [1–9], promising novel opportunities for applications in nanoscience and nanotechnology. In particular, impressive properties of small gold clusters have been demonstrated in the field of catalysis [10, 11], plasmonics [12], biosensing and medical applications [13–15]. Concerning optical properties, the reduction of a nanoparticle's size eventually leads to transformation of the plasmonic absorption band to a set of discrete molecular-like energy levels, which do not scale with the cluster size, but strongly depend on the number of atoms [4] and the cluster structure [16]. Moreover, the relaxation dynamics of the optically excited clusters and the processes taking place in the excited states alter significantly with cluster size, surrounding, excitation energy and are still largely unexplored.

One of the widely used techniques to study the ultrafast relaxation dynamics of mass-selected clusters is the femtosecond time-resolved photoelectron spectroscopy (TRPES) [17–19]. The photoelectron spectra are sensitive both to nuclear motion and to electron configuration and thus can provide valuable information about the excited state lifetimes and dynamics. The main steps of the TRPES experiment are the following: First, a pump pulse promotes an atom or molecule to an excited state inducing coupled electron-nuclear dynamics. Subsequently, a photoelectron is detached by a probe pulse coming with some time delay after the pump pulse. By measuring the kinetic energy of the photoelectron the information on the current excited state energy is obtained and by adjusting the time delay the temporal evolution of the excited state can be investigated. This method has successfully been applied to a large variety of systems ranging from organic molecules and bio-chromophores [20, 21] to metallic and molecular clusters [22–27].

Although a measured TRPES contains information about nuclear and electron motion, additional theoretical information is necessary to establish the correspondence between the nuclear configuration, electronic excited state and the resulting kinetic energy of a detached photoelectron. Therefore, a method to simulate coupled electron-nuclear dynamics in a manifold of nonadiabatically coupled excited states under an external laser field action is required. Recently, the field-induced surface hopping (FISH) method has been developed

[28, 29] and implemented in the frame of the linear-response time-dependent density functional theory (TDDFT). This allowed for simulation of TRPES [25, 30, 31] and time-resolved harmonic generation signals in metal clusters [7].

Recently it has been experimentally demonstrated that the excited state relaxation dynamics as well as the fragmentation processes in Au_3^- clusters are strongly affected by a number of water molecules interacting with the cluster [26]. The experiment showed that the excited state lifetime decreased monotonously with the number of water molecules. Interestingly, in the experiment for the bare gold cluster and the cluster with only one water molecule adsorbed, photoelectron peaks corresponding to the gold cluster fragments Au^- and Au_2^- were observed at long time delays between pump and probe pulses. The time constants for cluster fragmentation differed in the two cases by approximately a factor of 66. In contrast, if two or more water molecules were attached to the cluster, no fragments of the cluster were seen. This effect attracts attention since it opens a possibility not only to control the excited state lifetimes of some small noble-metal anionic clusters by water adsorption, but also to govern the photo-dissociation processes and their time scales.

In the current contribution we combine experimental TRPES measurements with the mixed quantum-classical nonadiabatic dynamics in order to reveal the mechanism behind the above mentioned experimental findings and to systematically explore the influence of water solvation on excited state dynamics of gold clusters.

II. METHODS

A. Theoretical approach

For the simulation of dynamics and TRPE spectra of small gold clusters and their complexes with water molecules the following methodology was used. The coupled electron-nuclear dynamics under explicit pump pulse excitation was simulated using our FISH method, which was presented in detail elsewhere [28, 29]. Briefly, the FISH method is based on the propagation of a swarm of classical trajectories in the manifold of excited electronic states $E_i(\mathbf{R}(t))$, calculated "on the fly" for given nuclear coordinates $\mathbf{R}(t)$. Parallel to the trajectory propagation the expansion coefficients $C(t)$ of the electron wave function within this manifold of

states are determined by solving the Schrï¿œdinger equation

$$i\hbar\dot{C}_i(t) = E_i(\mathbf{R}(t))C_i(t) - \sum_j \left(\boldsymbol{\mu}_{ij}(\mathbf{R}(t)) \cdot \boldsymbol{\varepsilon}(t) + i\hbar D_{ij}(\mathbf{R}(t))\right) C_j(t). \quad (1)$$

In this approach, the electronic states are coupled to each other via the external laser field $\boldsymbol{\varepsilon}(t)$ as well as due to the nonadiabatic coupling $D_{ij}(\mathbf{R}(t))$, which allows for the description of both laser-driven electron dynamics due to single- and multi-photon absorption [32] and nonradiative relaxation processes.

Each classical trajectory is propagated under the action of the forces obtained from the energy gradient of the electronic state on which the trajectory "resides" at the current instant of time. Hopping between different electronic states occurs stochastically with probabilities being proportional to the rates of change of the electronic population $\rho_{ii} = C_i^* C_i$ of these states:

$$P_{i\to j} = P_{i,depopulation} P_{j,population} = \Theta(-\dot{\rho}_{ii}) \frac{-\dot{\rho}_{ii}}{\rho_{ii}} \Theta(\dot{\rho}_{jj}) \frac{\dot{\rho}_{jj}}{\sum_k \Theta(\dot{\rho}_{kk})\dot{\rho}_{kk}} \Delta t. \quad (2)$$

Here, the Θ-functions ensure that the hopping probability is nonzero only for initial states with decreasing electron population and for final states with increasing electron population based on the results of solving Eq. (1).

Thus, the necessary ingredients needed to carry out the trajectory propagation are the electronic excited state energies and their gradients, which in the current study are obtained using TDDFT due to its efficiency and satisfying accuracy for the systems under investigation. Other essential quantities, such as transition dipole moments and nonadiabatic couplings between different excited states can be also obtained in the framework of TDDFT as described in Ref. [7]. In the current simulations the linear response TDDFT with the gradient-corrected Perdew-Burke-Ernzerhof (PBE) exchange-correlation functional [33] was used together with the triple zeta valence plus polarization atomic Gaussian basis set (TZVPP) [34] and the relativistic 19 electron effective core potential for gold [35]. Preliminary calculations revealed that at this level of theory minimal energy nuclear geometries and absorption spectra of both anionic Au_3^- and neutral Au_3 clusters reproduced the results of experiments [36] and high-level theoretical calculations [37, 38] accurately enough. In Fig. 1 the absorption spectra calculated at TZVPP/PBE level of theory are presented in comparison with the ones obtained using the more accurate Coulomb-attenuated B3-LYP

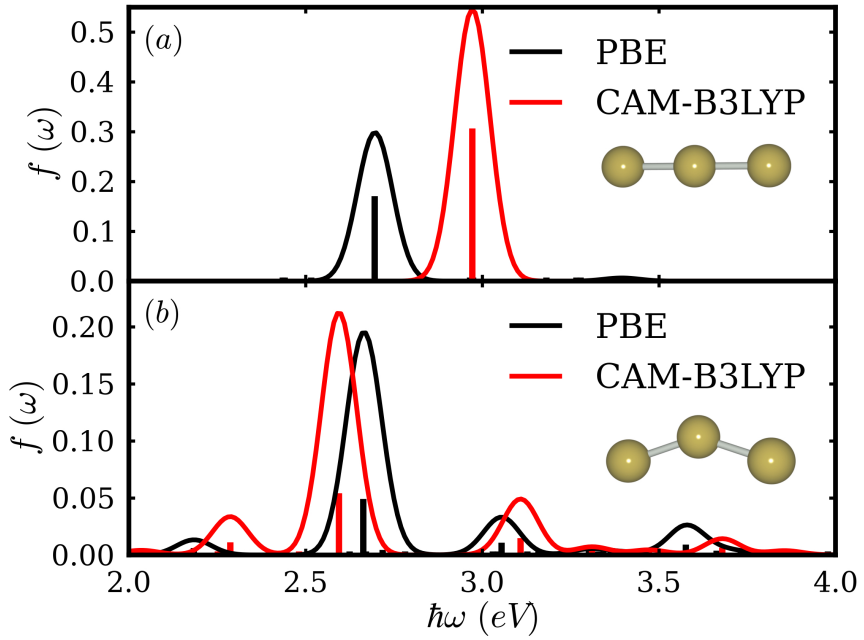

Figure 1: The absorption spectra of (a) the anionic Au_3^- and (b) the neutral Au_3 clusters calculated employing PBE and CAM-B3LYP functionals. In insets minimal energy structures obtained using PBE functional are presented.

(CAM-B3LYP) functional [39]. Nuclear configurations corresponding to the minimal energy isomers are shown in Fig. 1 as well. It is seen, that the shape and relative intensities of absorption lines are reproduced correctly using PBE functional.

Parallel to the trajectory propagation, the photoelectron signal is simulated. At each selected time instant τ the nuclear coordinates $\mathbf{R}(\tau)$ are extracted and used to calculate molecular orbitals and excited state energies for the anionic (A) and neutral (N) species. These are used to construct the approximate electronic wave functions of these species. The ground state electron wave functions for both species are represented by the Slater determinants $\left|\Phi_0^{A,N}(\tau)\right\rangle$ constructed from the occupied Kohn-Sham (KS) orbitals. The K-th excited state electron wave function for the anionic species $|\Psi_K^A(\mathbf{R}(\tau))\rangle$ is approximated by the configuration interaction singles-like expansion (CIS):

$$|\Psi_K^A(\mathbf{R}(\tau))\rangle = \sum_{a,r} c_{ar}^K \left|\Psi_{ar}^{CSF}\right\rangle . \tag{3}$$

where$\left|\Psi_{ar}^{CSF}\right\rangle$ represents a singlet spin-adapted configuration state function (CSF) defined

as:

$$|\Psi_{ar}^{CSF}\rangle = \frac{1}{\sqrt{2}}\left(|\Phi_a^r\rangle + \left|\Phi_{\bar{a}}^{\bar{r}}\right\rangle\right) \tag{4}$$

and $|\Phi_a^r\rangle$ and $|\Phi_{\bar{a}}^{\bar{r}}\rangle$ are the Slater determinants in which one electron has been promoted from the occupied orbital a to the virtual orbital r with spin α or β, respectively. The expansion coefficients c_{ar}^K in Eq. (3) can be determined based on the requirement that the wave function in Eq. (3) leads to the same density response as the one obtained by the linear response TDDFT procedure. Thus, for non-hybrid functionals without Hartree-Fock exchange the coefficients c_{ar}^K giving rise to mutually orthogonal electronic states are given by:

$$c_{ar}^K = \left(\frac{\epsilon_r - \epsilon_a}{\omega_K}\right)^{-1/2} (X_{ar}^K + Y_{ar}^K)\,, \tag{5}$$

where ϵ_a and ϵ_r are the orbital energies of a-th occupied and r-th virtual single electron orbitals, respectively, and X^K and Y^K represent the solution of the TDDFT eigenvalue problembd [40, 41]. The excited state electron wave function $|\Psi_K^N(\mathbf{R}(\tau))\rangle$ for the neutral species, which is an open-shell system, is approximated by the following expansion:

$$|\Psi_K^N(\mathbf{R}(\tau))\rangle = \sum_{a,r} c_{ar}^{\alpha K}\,|\Phi_a^r\rangle + \sum_{\bar{a},\bar{r}} c_{\bar{a}\bar{r}}^{\beta K}\,|\Phi_{\bar{a}}^{\bar{r}}\rangle\,. \tag{6}$$

The expansion coefficients are calculated in the same manner as in Eq. (**??**), the indices a ($\bar{a}$) run over all occupied and r ($\bar{r}$) over all virtual KS orbitals with spin α (β). It is worth noting that the sets of molecular orbitals used for construction of the Slater determinants differ for the anion and neutral species and thus the orbital relaxation effects are included.

The anion is assigned an electronic energy $E_K^A(\mathbf{R}(\tau))$ and a wave function $|\Psi_K^A(\mathbf{R}(\tau))\rangle$ depending on the electronic state in which the selected trajectory resides at the current instant of time, while for the neutral species all the excited states below $E_K^A(\mathbf{R}(\tau)) - E_0^N(\mathbf{R}(\tau)) + \hbar\omega_{probe}$ are taken into account. The Dyson orbital corresponding to the electron detachment from the anionic state $|\Psi_K^A(\mathbf{R}(\tau))\rangle$ with the resulting neutral species in the state $|\Psi_L^N(\mathbf{R}(\tau))\rangle$ is determined as follows:

$$\left|\varphi_{K,L}^D(\tau)\right\rangle = \sqrt{n}\,\langle\Psi_L^N(\mathbf{R}(\tau))\,|\Psi_K^A(\mathbf{R}(\tau))\rangle\,. \tag{7}$$

Here n is the number of electrons in the anionic species. The overlap integral in (7) can be reduced to the overlap between molecular orbitals of neutral and anionic species, which can

be further calculated using standard quantum-chemical routines [42]. The maximal kinetic energy of the ejected electron can be estimated as

$$E^{kin}_{K,L}(\tau) = \hbar\omega_{probe} + E^{A}_{K}(\mathbf{R}(\tau)) - E^{N}_{L}(\mathbf{R}(\tau)), \tag{8}$$

and the intensity of the electron signal is assumed to be proportional to the square of the corresponding Dyson orbital (7). Thus the TRPES of each trajectory is calculated as a sum over all electronic states of the neutral species. The energy distribution around $E^{kin}_{K,L}(\tau)$ is assumed to be Gaussian:

$$S\left(E,\tau\right) = \sum_{L} \left\|\varphi^{D}_{K,L}(\tau)\right\|^{2} \exp\left(-\frac{\left(E - E^{kin}_{K,L}(\tau)\right)^{2}}{2\sigma^{2}}\right). \tag{9}$$

In the described manner the photoelectron spectra are calculated along each trajectory. The final TRPES is obtained after averaging of the single-trajectory spectra over the whole ensemble.

B. Experimental setup

The experimental methods and setup are described in detail elsewhere [43]. Briefly, hydrated gold anion particles were produced in a pulsed arc cluster ion source and mass-selected using a time-of-flight mass spectrometer. Since the clusters spent sufficiently long time in a water-cooled extender for thermalization, the temperature of the clusters was estimated to be the room temperature. A selected bunch of clusters was irradiated by two successive laser pulses generated by a Ti:sapphire laser system. The second (3.11 eV) and third (4.66 eV) harmonics of the fundamental mode were used as pump and probe pulses, respectively. The full width at half maximum of the both pulses was approximately the same and equal to 30 meV. The instrumental time resolution was determined by measuring the cross-correlation function of the pump and probe pulses to be ∼240 fs. Under the pump pulse action a certain fraction of anionic clusters was excited and afterwards the probe pulse detached a photoelectron from an anion in the ground or excited state. Consequently, the kinetic energy of photoelectrons was measured using a "magnetic bottle" type time-of-flight electron spectrometer.

III. RESULTS AND DISCUSSION

A. Au_3^-

The bare Au_3^- cluster was used as a benchmark system to validate the theoretical methods and to calibrate the experimental setup. The simulations of Au_3^- excited state dynamics induced by an external laser pulse were carried out for an ensemble consisting of 100 trajectories. The initial conditions for each trajectory were generated using the Wigner distribution [44] at 300 K temperature based on the optimized linear structure of Au_3^-. The pump pulse was assumed to have a Gaussian temporal profile with the peak intensity (2.6×10^9 V·m^{-1}) and FWHM (138 fs) to reproduce the experimental values. All the 13 excited states below the theoretical vertical detachment energy (VDE) of 3.6 eV were included in the simulations. During the pump pulse action 98% of trajectories "hopped" between the ground and excited electronic states due to the electric field coupling. After the pulse had ceased 52% of trajectories remained in the high excited states (S_9-S_{13}) while the rest of ensemble was in the ground state. The electron population dynamics of the ensemble of trajectories is presented in Fig. 2 (a). It is seen, that within 1 ps of simulation time only relaxation to the states $S_{9,10}$ from the higher-lying electronically excited states occurs, but no relaxation back to the ground electronic state of Au_3^- is observed. This can be explained by the relatively large energy gap between the manifold of states S_9- S_{13} and the lower-lying excited states (cf. Fig. 2(b)). The results are in correspondence with the experimental observation of a long excited state lifetime in the bare Au_3^- cluster, which was measured to be 1.6 ns. During the simulations time no dissociation of the Au_3^- clusters was observed, which is also in agreement with the experimental data.

TRPE spectra were calculated for every trajectory in the ensemble as described in Sec. II A and averaged afterwards. The final spectrum was shifted by 0.3 eV to the lower energies to account for the difference between the experimental (3.9 eV) and theoretical (3.6 eV) VDEs of Au_3^-. The comparison between theoretical and experimental results is presented in Fig. 3. The central panel (b) shows the theoretical TRPES obtained for the simulation time of 1 ps. The left panel (a) shows the experimental spectrum recorded for the non-excited ensemble (the time delay between pump and probe pulses is negative) and the right panel shows the experimental results for the relatively large time delay. The two broad time-dependent peaks

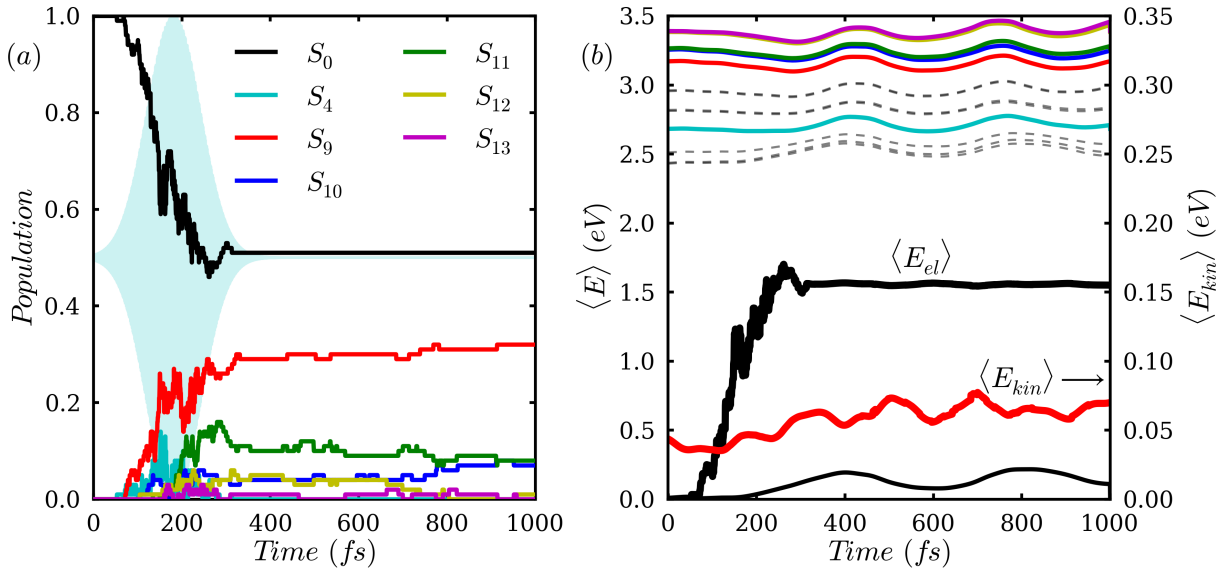

Figure 2: (a) The population dynamics of the Au_3^- ensemble induced by the experimental pump pulse. The pump pulse is shown on the background; (b) the temporal evolution of the ground and excited electronic state energies of Au_3^- (thin lines, left axis), averaged over the ensemble of trajectories, with the dashed lines showing the non-populated excited states, the average electronic energy (thick black line, left axis) and the average nuclear kinetic energy of the Au_3^- ensemble (thick red line, right axis).

X and X* absent at negative time-delay are attributed to the photo-detachment of electrons from the Au_3^- excited states $S_9 - S_{13}$ with the neutral species Au_3 created in the ground (X) and low-lying excited (X*) states. These peaks exhibit oscillations due to vibrational motion of the Au_3^- clusters.

The time-independent peaks of moderate intensity A, B, and C (see Fig. 3 (b)) arise from the photo-detachment of an electron by two pump photons with the neutral species in the ground (A), $D_1 - D_3$ excited (B) and $D_4 - D_5$ excited (C) state. Some of these peaks can be distinguished in the experimental spectra at negative (A, B) and positive (B) time delays. The intense peaks D, E, and F in the low-energy region correspond to the photo-detachment of an electron by the probe pulse only from the ground state of Au_3^- to the the ground (D), $D_1 - D_3$ excited (E), and $D_4 - D_5$ excited (F) states of the neutral species. In the experimental spectra these peaks are well distinguishable at both negative and positive time delays. Unlike the peaks A - C, these peaks slightly oscillate with time due to coherent

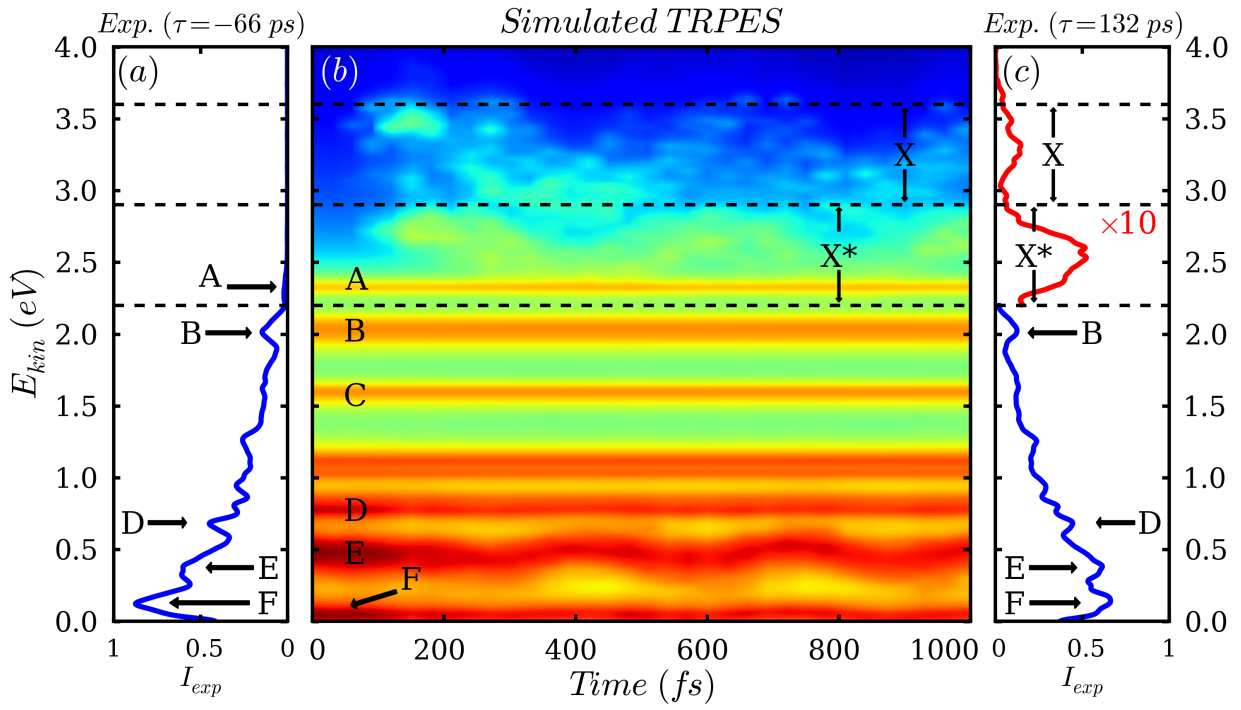

Figure 3: The photoelectron spectra of the Au_3^- (a) measured at the negative time delay between the pump and probe pulses of τ=-66 ps, (b) the simulated time-resolved spectrum for time delays ranging from 0 to 1 ps, the intensity of the signal is denoted with the color, (c) experimental PES at the large positive time delay of 132 ps. The part of the spectrum above 2.2 eV denoted with red color is 10 times magnified.

vibrational motion of Au_3^- induced by the pump pulse. The decrease of intensity of these peaks after ∼300 fs is due to depopulation of the ground state by the pump pulse (cf. Fig. 2 (a)).

In general, on the benchmark system Au_3^- it was demonstrated that the theoretical approach allows for describing of time-resolved photoelectron spectra including the signal of electrons detached by two pump pulse photons.

B. $Au_3^-H_2O$

In order to determine the global minimum energy structure of the $Au_3^-H_2O$, a molecular dynamics in the ground state was carried out for 8 ps. Starting from 1 ps of the simulation time the coordinates were taken with a time step of 70 fs and optimized. All the structures

converged to the same minimal energy configuration shown in Fig. 4 (a). This configuration was subsequently used to generate 100 initial conditions for the FISH dynamics under the action of the experimental pump pulse. The initial structures and velocities were generated using the Wigner distribution at room (300 K) temperature. In the dynamics simulations all the electronic excited states below the VDE at the selected TZVPP/PBE level of theory (3.92 eV) were taken into account. In this energetic region there are 17 excited electronic states, which form the density of states (DOS) shown in Fig. 4 (b). For better visualization of the population dynamics the manifold of the excited states is divided into three regions shaded in Fig. 4 (b) with different colors. The central "red" region contains the most intense absorption peak of the $Au_3^-H_2O$, and the electronic state resonant to the pump pulse. The "blue" and "green" regions contain lower- and higher-energy electronic states, respectively.

During 3 ps of the dynamics simulations the following fragmentation processes have been observed:

(i) $Au_3^-H_2O \rightarrow Au_3^- + H_2O$ (29% of trajectories, 16% fragmented in the excited and 13% in the ground state);

(ii) $Au_3^-H_2O \rightarrow Au^- + Au_2H_2O$ (6% of trajectories, in the excited state);

(iii) $Au_3^-H_2O \rightarrow Au^-H_2O + Au_2$ (2% of trajectories, in the excited state);

(iv) $Au_3^-H_2O \rightarrow OH^- + Au_3H$ (1% of trajectories, in the ground state).

It should be noted that due to the moderate number of trajectories in the ensemble we can not accurately predict the branching ratio of these fragmentation processes based on the current simulations. However, it is clear that these reaction paths are possible in the system under consideration as a result of excitation by the experimental laser pulse.

The electronic population dynamics of the $Au_3^-H_2O$ ensemble is presented in Fig. 4 (c). The color lines represent the total population of all electronic states from the energy regions shaded with the corresponding colors in Fig. 4 (b). Under the pump pulse action first the central energy region S_4-S_9 is populated, but a significant part of the electron population is further transferred to the higher-lying states S_{10}-S_{17} due to the multi-photon absorption. Finally, after the pump pulse has ceased, the relaxation of the electronic population to the lowest excited states S_1-S_3 occurs. In contrast to the bare Au_3^- cluster, parallel to the electronic relaxation within the manifold of the excited states, a significant population

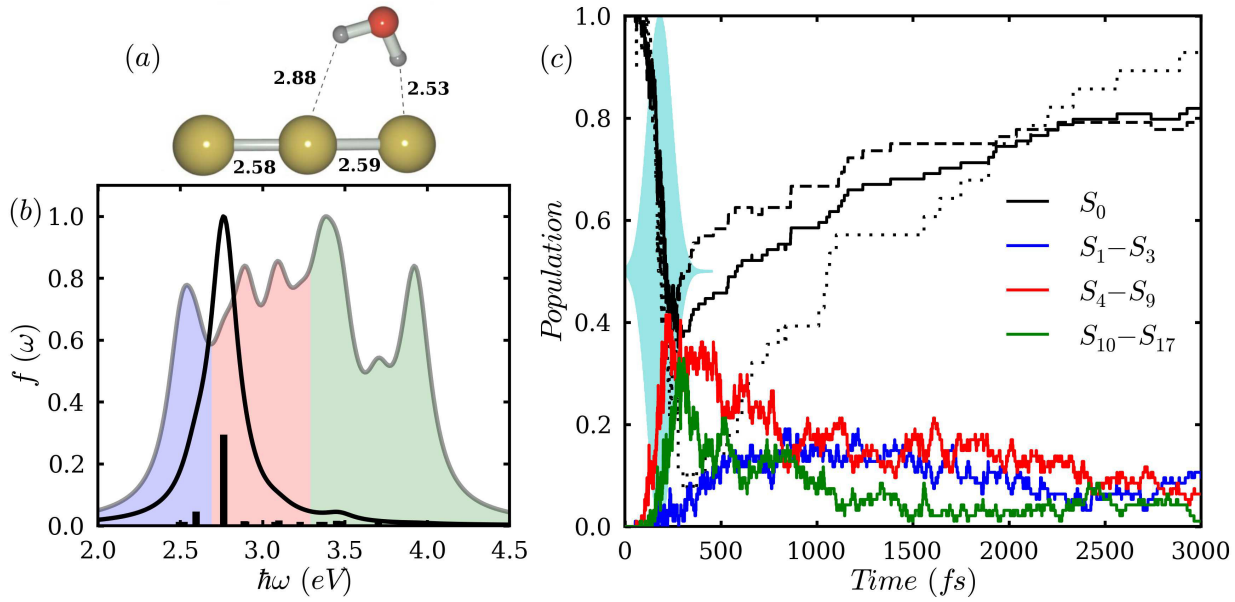

Figure 4: (a) The minimal energy structure of an Au_3^- cluster with one water molecule. The distances between atoms in ï¿œngstrï¿œm are given; (b) the absorption spectrum (shown with the solid black line) and the density of states (the semi-transparent filled line on the background) of the optimized structure. The manifold of excited states is divided into three regions, the corresponding area under the DOS line is shaded with different colors; (c) the population dynamics of the $Au_3^-H_2O$ ensemble induced by the experimental pump pulse presented on the background. The color lines show the electron population of the energy regions, marked in (b) with the corresponding colors, (dashed line) the ground state population of the sub-ensemble of trajectories which do not fragment in the excited state, (dotted line) the ground state population of the sub-ensemble of trajectories fragmenting in the excited state.

transfer to the ground state is observed. In order to determine the underlying mechanism, the ensemble of trajectories was divided into two sub-ensembles: the trajectories fragmenting in the excited state and those which do not show fragmentation in the excited state. The ground state electronic population of this two sub-ensembles is shown in Fig. 4 (c) with the dotted and dashed lines, respectively. It is clearly seen, that both of the sub-ensembles exhibit population transfer to the ground state with different time constants. Thus we conclude, that two competing processes are responsible for the population transfer back to the ground state, namely, fragmentation with the excess of energy used for separation of fragments (see Fig. 4(c), dotted line), and nonradiative relaxation with the excess of energy

transferred to the vibrational motion of the molecule (Fig. 4(c), dashed line). The results of the simulation show, that the latter process can ultimately lead to fragmentation along paths (i) or (iv), but does not lead to dissociation of the gold cluster itself.

In the simulations the fragmentation of gold clusters occurred only in the excited state. A typical trajectory following the fragmentation path (ii) is presented in Fig. 5. In Fig. 5 (a) the evolution of the excitation energies of the selected trajectory is presented. At selected time moments (285, 615, 840, 1100, and 1450 fs) the snapshots of the nuclear configuration and excited state electron density difference to the ground state are taken and presented in Fig. 5 (c). The semi-transparent thick red line shows the actual electronic state of the trajectory. It is seen, that under the action of the external laser pulse the trajectory is promoted to the excited state S_9, from which it quickly decays to the state S_8 denoted in Fig. 5 (a) with the solid green line. In this state the trajectory resides for ∼500 fs and afterwards through several intermediate states it decays to the S_2 state (shown with the solid blue line). Unlike the higher-energy excited states, in which the trajectory resided before, this state is characterized by a strongly asymmetric electron density difference to the ground state, meaning that the excited electron is mainly localized around the right gold atom. Additionally, the decrease of the electron density in the region between the central and the right atoms is clearly seen at 840 and 1100 fs (cf. the blue spots in the corresponding snapshots in Fig. 5 (c)). As a result, the Au_3^- cluster dissociates into the neutral Au_2 and anionic Au^- fragments. The charge distribution is analyzed by calculating partial atomic charges of each gold atom during the dynamics presented in Fig. 5 (b). The partial charges were calculated using the CHelpG algorithm [45]. It follows from the figure, that as a result of the dynamics in the S_2 state, the negative charge is transferred to the third (right) gold atom.

Therefore we can assume that the dissociation of the Au_3^- cluster occurs due to promotion to a weakly-bound excited state. Indeed, a test nonadiabatic dynamics simulation on a bare Au_3^- cluster starting from the S_2 state revealed, that the bare cluster dissociates in this state into the neutral Au_2 and anion Au^- as well. In the minimal energy structure this state is dark for both $Au_3^-H_2O$ (cf. Fig. 4 (b)) and bare Au_3^- and thus can not be directly populated by a laser pulse, but can be reached through nonadiabatic processes during excited state dynamics. The value of nonadiabatic coupling between the excited

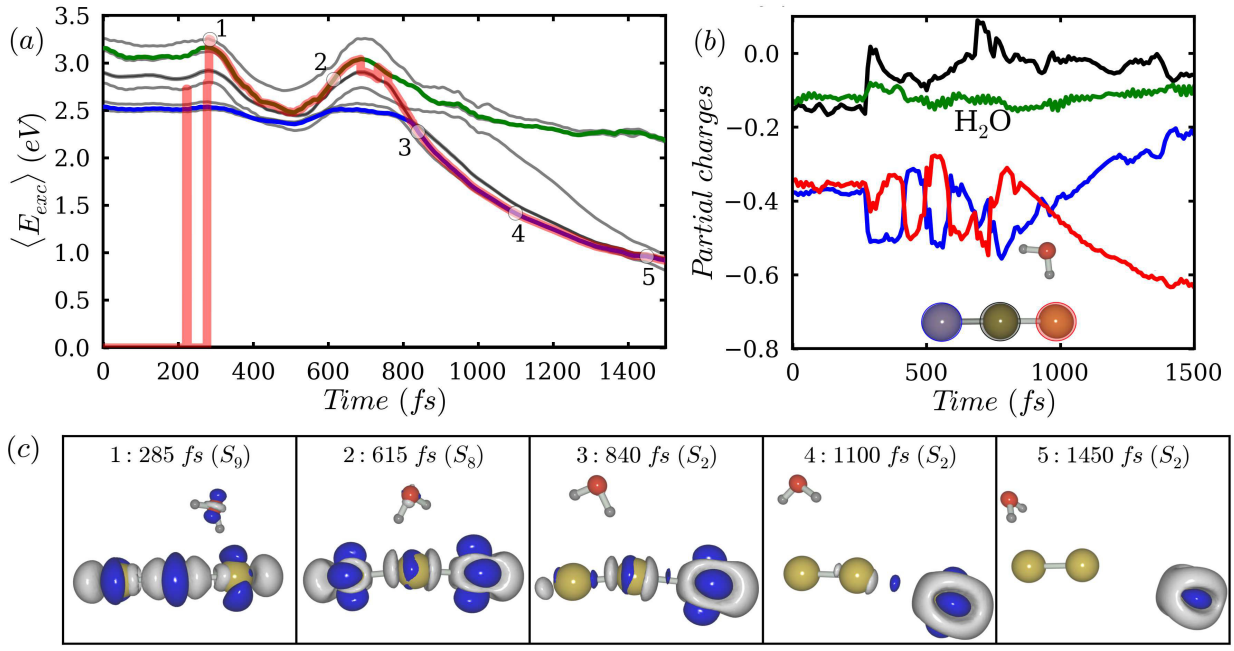

Figure 5: (a) The excitation energies of the $Au_3^-H_2O$ molecule along a selected trajectory. With the solid lines the excitation energies to the S_2 (blue) and S_8 (green) states are shown. The thick semi-transparent red line shows the current state of the trajectory. The numbers 1-5 denote the time instants at which the snapshots presented in (c) are taken; (b) the partial charges of the gold atoms and water in the $Au_3^-H_2O$ molecule calculated along the selected trajectory. The lines are colored according to the scheme shown in inset, which corresponds to the nuclear configuration at 285 fs of simulation time; (c) the snapshots taken at 285, 615, 840, 1100, and 1450 fs of the simulation time representing the actual nuclear configuration and the electron density difference between the current excited and the ground electronic states (increase of the electron density is shown with white and decrease with blue colors). The actual excited state is given in brackets.

states in our approach determines the probability and consequently the rate of population transfer to the "dissociative" state. Due to the presence of a water molecule the nonadiabatic coupling of the high-lying excited states to the S_2 state is much higher than that in the bare Au_3^- cluster, leading to faster population of this state and cluster dissociation as compared to a bare cluster.

The simulated TRPE spectrum of the $Au_3^-H_2O$ is presented in Fig. 6 and compared to the experimental PES measured at zero time delay and positive time delays of τ = 1.3

ps and τ = 125.5 ps. At zero time delay the clusters are in the ground state and in the photoelectron spectra only peaks A - D arise due to two-pump-photon (A - C) and probe-only (D) photo-detachment. The peak B, which is clearly seen in the simulated TRPES but absent in the measured PES is attributed to the photo-detachment by two pump pulse photons with the neutral species created in the D_{1-3} excited states. This states have the charge-transfer character and thus the excitation energy is underestimated at the PBE level of theory. Calculations using the more accurate CAM-B3LYP functional reveal, that these excited states should be 0.6 eV higher in energy. This would lead to the shift of the peak B to lower kinetic energy and as a result to overlap with the peak C. The same deficiency is observed for the $Au_3^-[H_2O]_2$ as well.

At positive time delays several time-dependent features are observed. The signal in the region Y comes from the photoelectrons detached from the $Au_3^-H_2O$ molecules being in the high excited states S_{10}-S_{17}. The signal is weak and almost not seen in the experiment, moreover, it vanishes within 1 ps as the population of this electronic states decays (see. Fig. 4 (c)). The peaks X and X* correspond to the photo-detachment from the $Au_3^-H_2O$ in the S_4-S_9 excited states with the neutral product formed in the ground and low-lying excited states, respectively. Additionally, at later times such trajectories contribute to these peaks, which have fragmented following the path (i), i.e. lost the water molecule. Finally, the peak X** arises due to the photo-detachment of the $Au_3^-H_2O$ in the S_1-S_3 excited states with the neutral product formed in the ground state. This peak appears later than the X and X* peaks as the corresponding manifold of states is populated (cf. Fig. 4 (c)). A sharp feature appearing after ∼1.3 ps of the simulation time corresponds to the signal from the Au^- anion, which is a product of the trajectories fragmenting along paths (ii) and (iii). It is complicated to distinguish this signal in the experiment at moderate time delays due to overlap with the peaks X* and X**, but at relatively large time delays this peak is clearly seen (cf. Fig. 6 (c), green line). Another feature appearing at large time delays is the signal at $\sim$ 2.7 eV, which can be a trace of Au_2^-. This fragment has not been observed in the simulations, because the fragmentation path $Au_3^- \rightarrow Au_2{}^- +$ Au is energetically unfavorable. It is worth noting, that at 125 ps time delay no signal from the excited states of $Au_3^-H_2O$ is observed (see region X in Fig. 6 (c)) which confirms the shorter lifetimes of the excited states as compared to the bare Au_3^- cluster (see regions X and X* in Fig. 3 (c)).

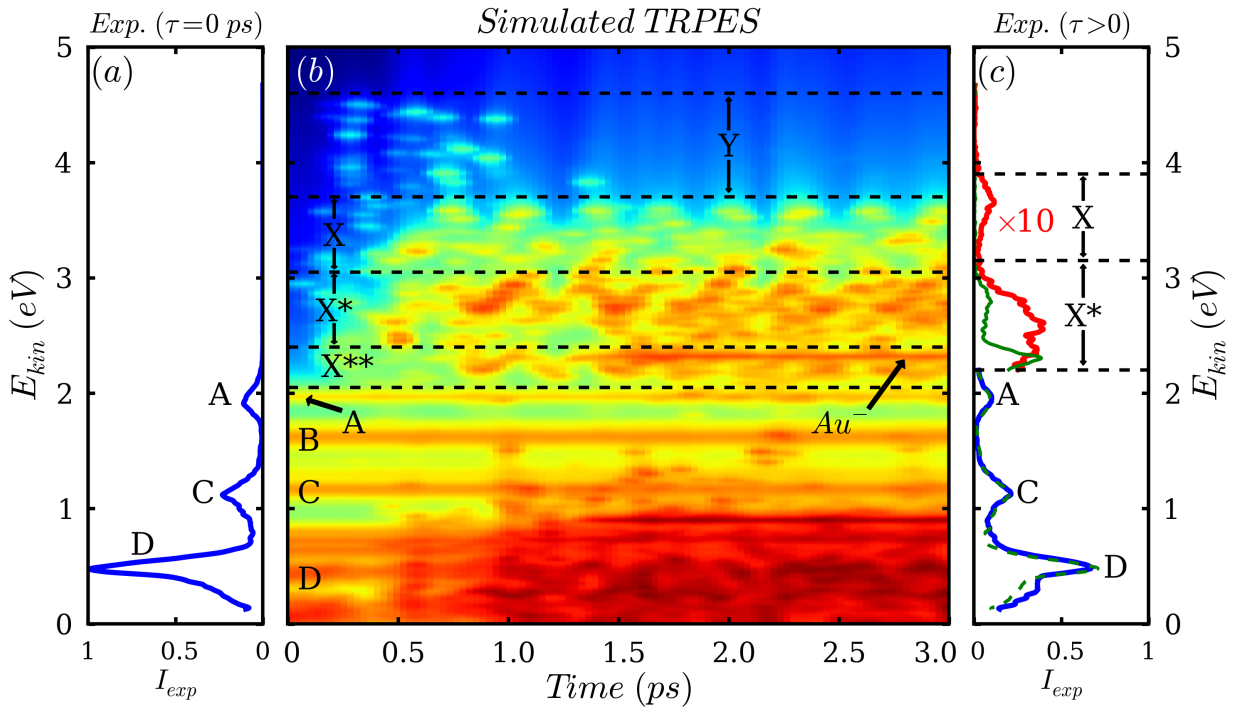

Figure 6: The photoelectron spectra of the $Au_3^-H_2O$ ensemble (a) measured at the zero time delay between the pump and probe pulses, (b) the simulated time-resolved spectrum for time delays ranging from 0 to 3 ps, the intensity of the signal is denoted with the color, (c) measured at the positive time delays of 1.3 ps (blue and red lines, the red line corresponds to the signal multiplied by 10 as compared to the blue line) and of 125.5 ps (green dashed and solid lines, the solid green line is multiplied by 10).

C. $Au_3^-[H_2O]_2$

A search for a global minimal energy structure of $Au_3^-[H_2O]_2$ has been performed in the same manner as described in Section III B. Several stable isomers have been found, the energy difference between the lowest-energy and second-to-lowest energy isomers being ∼0.1 eV. According to the Boltzmann distribution the population of higher-energy isomers at room temperature is small (∼2%) and therefore we focus only on the lowest-energy one. The nuclear configuration of this isomer is presented in Fig. 7 (a). This structure was used to generate 50 initial conditions for an ensemble of trajectories by sampling the Wigner distribution at room temperature. The dynamics simulations using the FISH method were carried out within a manifold of the ground and 15 excited electronic states. The DOS of

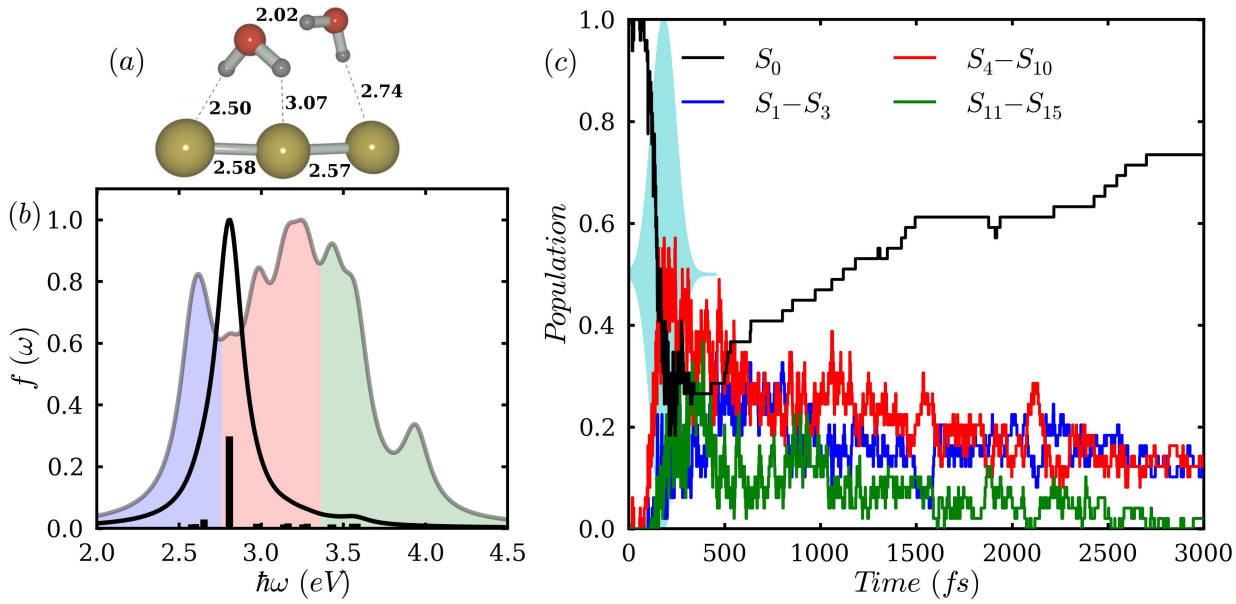

Figure 7: (a) The minimal energy structure of an $Au_3^-[H_2O]_2$ molecule. The distances between atoms in ï¿œngstrïï¿œm are given; (b) the absorption spectrum (shown with the solid black line) and the density of states (the semi-transparent filled line on the background) of the structure in (a), the manifold of the excited states is divided into three regions, the corresponding area under the DOS line is shaded with different colors; (c) the population dynamics of the $Au_3^-[H_2O]_2$ ensemble induced by the experimental pump pulse shown in the background, the color lines show the electron population of the energy regions, marked in (b) with the corresponding colors.

the electronic state manifold taken into account in the simulations is presented in Fig. 7 (b) together with the absorption spectrum of the lowest-energy isomer. For better visualization of the population dynamics, the manifold of excited states was divided into several regions shaded in Fig. 7 (b) with different colors. The central "red" region contains the most intense absorption peak and is resonant to the pump laser pulse. The "blue" and "green" regions contain the excited states below and above the central region, respectively.

During the 3 ps of simulation time the following fragmentation paths have been observed:

(i) $Au_3^-[H_2O]_2 \rightarrow Au_3^-H_2O + H_2O$ or $Au_3^- + 2H_2O$ (30% of trajectories, all fragmented in the ground state);

(ii) $Au_3^-[H_2O]_2 \rightarrow Au_2OH^- + AuH + H_2O$ (2% of trajectories, in the ground state).

It is worth noting, that all the fragmentation processes occurred after a trajectory relaxed

back to the ground state. Moreover, only one trajectory showed the dissociation of the gold cluster, which happened much after the trajectory decayed to the ground state.

The electronic population dynamics of the $Au_3^-[H_2O]_2$ ensemble is presented in Fig. 7 (c). As in the case of $Au_3^-H_2O$, under the pump pulse action first the central "red" region S_4-S_{10} is populated with subsequent promotion of a part of the population to the higher "green" region S_{11}-S_{15}. After the pump pulse ceases, the electron population is transferred down to the "red" and to the lowest-energy "blue" region. Additionally, a significant population transfer back to the ground state is observed. In contrast to the $Au_3^-H_2O$, the fragmentation processes do not contribute to this population decay. Thus we can conclude, that the fragmentation in the excited state is completely suppressed by the non-radiative relaxation to the ground state. This explains the low number of trajectories showing the dissociation of the gold cluster, because the ground state is much strongly bound than some of the lowest excited states and the excess of the kinetic energy is often not sufficient to cause the gold cluster dissociation.

Indeed, the existence of the weakly-bound states along the Au-Au bond stretching coordinate is proven by more accurate calculations employing CAM-B3LYP functional in $Au_3^-[H_2O]_n$, n=0...2. The results are presented in Fig. 8. In the calculations all the atoms except the right one (as shown in inset) were fixed and thus the energies do not correspond to the minimal energy paths, but the dissociative character of the lowest excited state is clearly seen.

Finally, we compare the simulated TRPES of the $Au_3^-[H_2O]_2$ ensemble to the experimental data (see Fig. 9). At zero time delays in the measured data as well as in the simulated ones only the peaks due to two-pump-photon (A-C) and probe-only (D) photo-detachment are observed. As a result of the pump pulse action the peak D is depleted (see Fig. 9 (b) at 0.3-0.4 ps) and the following time-dependent features appear: In the region X the signal is due to the photo-detachment of the $Au_3^-[H_2O]_2$ molecules in the S_4-S_{10} excited states with the neutral species created in the ground state. The signal in X* comes from the members of the ensemble residing in the lowest manifold of excited states S_1-S_3. Finally, the peak Y is due to the photoelectrons detached from the $Au_3^-[H_2O]_2$ molecules in the S_{11}-S_{15} excited states and decays within 1 ps of the simulation time as the population of the corresponding states decreases (cf. Fig. 7 (c)). In the panel (c) the experimental spectra taken at moderate

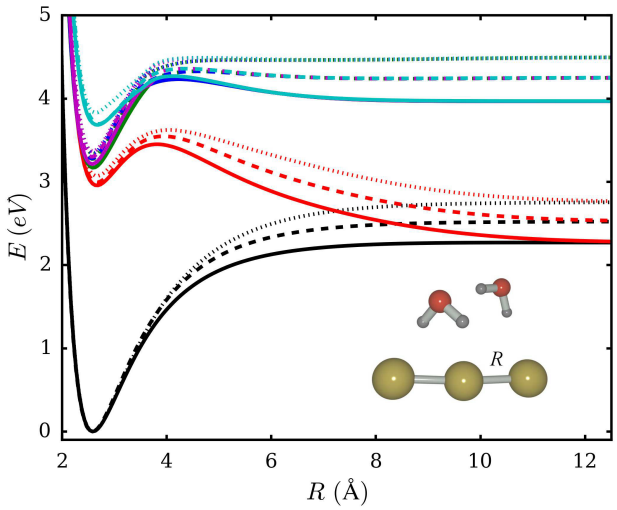

Figure 8: Evolution of the ground state and low excited state electronic energies of Au_3^- (solid lines), $Au_3^-H_2O$ (dashed lines), and $Au_3^-[H_2O]_2$ (dotted lines) with respect to the Au-Au bond stretching, as it is marked in inset for the $Au_3^-[H_2O]_2$ case. All the energies are plotted relatively to the ground state minimum of the given species.

time delay of 1.3 ps (blue and red lines) as well as at long time delay of 125 ps (green lines) are presented. At 1.3 ps the signal from $Au_3^-[H_2O]_2$ in the excited states is clearly seen (peaks X and X*), which significantly decays at later times. Notably, no signal from gold cluster fragments Au^- or Au_2^- is seen in the experiment at 125 ps time delay.

IV. CONCLUSION

In summary, we have studied both experimentally and theoretically the excited state dynamics and photo-dissociation of $Au_3^-[H_2O]_n$, n=0...2, clusters. The experimental TRPES shows that the excited state lifetime of bare Au_3^- cluster is 1.6 ns and as a result of the photo-excitation the cluster dissociates into Au^- + Au_2 or less probably into Au + Au_2^- fragments. When one water molecule is adsorbed on the Au_3^- cluster, the excited state lifetime decreases dramatically down to 24 ps, but the products of the gold cluster dissociation are still observed in the TRPES at longer time delays. If two or more water molecules are added to the Au_3^- cluster, the excited state lifetimes become even shorter (9.3 ps for $Au_3^-[H_2O]_2$ and 5.5 ps for $Au_3^-[H_2O]_3$), but no fragments of Au_3^- cluster are observed in the

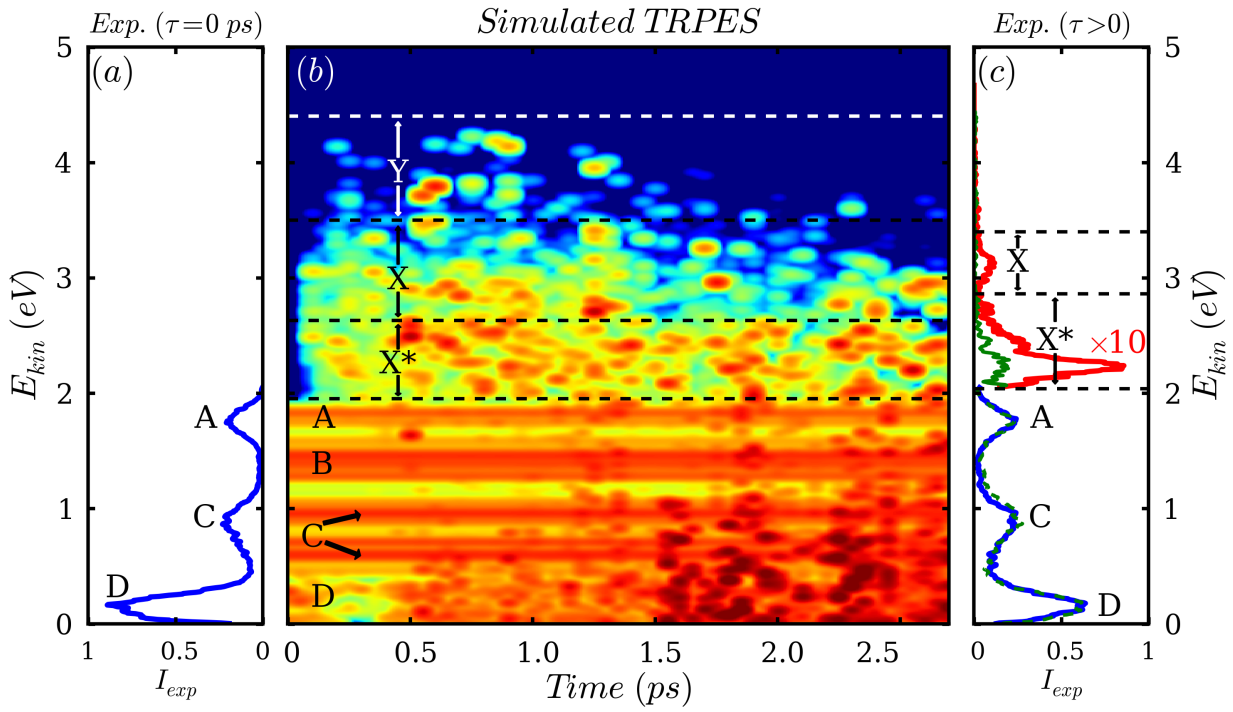

Figure 9: The photoelectron spectra of the $Au_3^-[H_2O]_2$ ensemble (a) measured at the zero time delay between the pump and probe pulses, (b) the simulated TRPES for time delays ranging from 0 to 2.7 ps, the intensity of the signal is denoted with the color code, (c) the photoelectron spectra measured at the positive time delays of 1.3 ps (blue and red lines, the part of the spectrum shown with the red line is multiplied by factor 10) and of 125.5 ps (green dashed and solid lines, the solid green line is multiplied by 10).

photoelectron spectra, which suggests that the photo-fragmentation is suppressed in this case by the water solvation effects.

The theoretical simulations reveal that two competing processes cause the excited state population decay, namely, dissociation of the gold cluster and non-radiative relaxation to the ground state with excess electronic energy redistributed among the vibrational degrees of freedom. The gold cluster dissociation occurs as a result of the nonadiabatic dynamics in the low-lying excited state. The probability and rate of cluster fragmentation are determined by the time required to reach this state and by the time spent in this state. The adsorption of water molecules on the gold anionic cluster decreases the time constant of relaxation within the excited state manifold. As a consequence the weakly-bound low-lying excited states are reached on a shorter time scale, but if the time constant is too small (as in the case of two

or more water molecules adsorbed) the subsequent relaxation to the ground state occurs faster leading to suppression of the gold cluster fragmentation. This explains the gradual decrease of excited state lifetimes with the number of adsorbed water molecules as well as the suppression of Au_3^- fragmentation when two or more water molecules are adsorbed.

---

[1] Bonačić-Koutecký, V.; Veyret, V.; Mitrić, R. *J. Chem. Phys.* **2001**, *115*, 10450–10460.

[2] Peyser, L.; Vinson, A.; Bartko, A.; Dickson, R. *Science* **2001**, *291*, 103–106.

[3] Kelly, K.; Coronado, E.; Zhao, L.; Schatz, G. *J. Phys. Chem. B* **2003**, *107*, 668–677.

[4] Zheng, J.; Zhang, C.; Dickson, R. *Phys. Rev. Lett.* **2004**, *93*.

[5] Lal, S.; Link, S.; Halas, N. J. *Nature Photon.* **2007**, *1*, 641–648.

[6] Johnson, G. E.; Mitrić, R.; Bonačić-Koutecký, V.; Castleman, A. W., Jr. *Chem. Phys. Lett.* **2009**, *475*, 1–9.

[7] Lisinetskaya, P. G.; Mitrić, R. *Phys. Rev. A* **2011**, *83*.

[8] Benson, O. *Nature* **2011**, *480*, 193–199.

[9] Lang, S. M.; Bernhardt, T. M. *Phys. Chem. Chem. Phys.* **2012**, *14*, 9255–9269.

[10] Sanchez, A.; Abbet, S.; Heiz, U.; Schneider, W.; Häkkinen, H.; Barnett, R.; Landman, U. *J. Phys. Chem. A* **1999**, *103*, 9573–9578.

[11] Daniel, M.; Astruc, D. *Chem. Rev.* **2004**, *104*, 293–346.

[12] Lee, K.-S.; El-Sayed, M. A. *J. Phys. Chem. B* **2006**, *110*, 19220–19225.

[13] Haes, A.; Van Duyne, R. *Expert Rev. Mol. Diagn.* **2004**, *4*, 527–537.

[14] Katz, E.; Willner, I.; Wang, J. *Electroanal.* **2004**, *16*, 19–44.

[15] Zharov, V.; Mercer, K.; Galitovskaya, E.; Smeltzer, M. *Biophys. J.* **2006**, *90*, 619–627.

[16] Huang, W.; Pal, R.; Wang, L.-M.; Zeng, X. C.; Wang, L.-S. *J. Chem. Phys.* **2010**, *132*.

[17] Pontius, N.; Bechthold, P.; Neeb, M.; Eberhardt, W. *Phys. Rev. Lett.* **2000**, *84*, 1132–1135.

[18] Stolow, A. *Annu. Rev. Phys. Chem.* **2003**, *54*, 89–119.

[19] Suzuki, T. *Annu. Rev. Phys. Chem.* **2006**, *57*, 555–592.

[20] Bisgaard, C. Z.; Satzger, H.; Ullrich, S.; Stolow, A. *ChemPhysChem* **2009**, *10*, 101–110.

[21] Suzuki, Y.-I.; Fuji, T.; Horio, T.; Suzuki, T. *J. Chem. Phys.* **2010**, *132*.

[22] Pontius, N.; Bechthold, P.; Neeb, M.; Eberhardt, W. *Appl. Phys. B* **2000**, *71*, 351–356.

[23] Stolow, A.; Bragg, A.; Neumark, D. *Chem. Rev.* **2004**, *104*, 1719–1757.

[24] Stanzel, J.; Burmeister, F.; Neeb, M.; Eberhardt, W.; Mitrić, R.; Bürgel, C.; Bonačić-Koutecký, V. *J. Chem. Phys.* **2007**, *127*.

[25] Stanzel, J.; Neeb, M.; Eberhardt, W.; Lisinetskaya, P. G.; Petersen, J.; Mitrić, R. *Phys. Rev. A* **2012**, *85*.

[26] Braun, C.; Proch, S.; Seo, H. O.; Kim, Y. D.; Ganteför, G. *Chem. Phys. Lett.* **2012**, *530*, 35–38.

[27] Braun, C.; Proch, S.; Kim, Y. D.; Ganteför, G. *Chem. Phys. Lett.* **2013**, *588*, 27–30.

[28] Mitrić, R.; Petersen, J.; Bonačić-Koutecký, V. *Phys. Rev. A* **2009**, *79*.

[29] Petersen, J.; Mitrić, R.; Bonačić-Koutecký, V.; Wolf, J.-P.; Roslund, J.; Rabitz, H. *Phys. Rev. Lett.* **2010**, *105*.

[30] Mitrić, R.; Petersen, J.; Wohlgemuth, M.; Werner, U.; Bonačić-Koutecký, V.; Wöste, L.; Jortner, J. *J. Phys. Chem. A* **2011**, *115*, 3755–3765.

[31] Mitrić, R.; Petersen, J.; Wohlgemuth, M.; Werner, U.; Bonačić-Koutecký, V. *Phys. Chem. Chem. Phys.* **2011**, *13*, 8690–8696.

[32] Röhr, M. I. S.; Petersen, J.; Wohlgemuth, M.; Bonačić-Koutecký, V.; Mitrić, R. *ChemPhysChem* **2013**, *14*, 1377–1386, NO PDF.

[33] Perdew, J.; Burke, K.; Ernzerhof, M. *Phys. Rev. Lett.* **1996**, *77*, 3865–3868, PBE functional.

[34] Schäfer, A.; Huber, C.; Ahlrichs, R. *J. Chem. Phys.* **1994**, *100*, 5829–5835, TZVP basis.

[35] Andrae, D.; Haußermann, U.; Dolg, M.; Stoll, H.; Preuß, H. *Theor. Chim. Acta* **1990**, *77*, 123–141, 19el ECP.

[36] Lecoultre, S.; Rydlo, A.; Félix, C.; Buttet, J.; Gilb, S.; Harbich, W. *J. Chem. Phys.* **2011**, *134*.

[37] Wesendrup, R.; Hunt, T.; Schwerdtfeger, P. *J. Chem. Phys.* **2000**, *112*, 9356–9362.

[38] Anak, B.; Bencharif, M.; Rabilloud, F. *RSC Adv.* **2014**, *4*, 13001–13011.

[39] Yanai, T.; Tew, D.; Handy, N. *Chem. Phys. Lett.* **2004**, *393*, 51–57, CAMB3LYP.

[40] Casida, M. E. In *Recent Advances in Density Functional Methods*; Chong, D. P., Ed.; Recent Advances in Computational Chemistry; World Scientific, Singapore, 1995; p 155.

[41] Dreuw, A.; Head-Gordon, M. *Chem. Rev.* **2005**, *105*, 4009–4037.

[42] Humeniuk, A.; Wohlgemuth, M.; Suzuki, T.; Mitrić, R. *J. Chem. Phys.* **2013**, *139*.

[43] Koyasu, K.; Niemietz, M.; Götz, M.; Ganteför, G. *Chem. Phys. Lett.* **2007**, *450*, 96–100.

[44] Wigner, E. *Phys. Rev.* **1932**, *40*, 749–759.

[45] Breneman, C. M.; Wiberg, K. B. *J. Comp. Chem.* **1990**, *11*, 361–373, ChelpG.